

Article

Kinematic Modelling and Experimental Validation of a Foldable Pneumatic Soft Manipulator

Zhuoqun Liu ¹, Xiang Zhang ^{1,2,*}, Hongwei Liu ², Yong Chen ¹, Yiyong Huang ² and Xiaoqian Chen ^{2,*}

¹ College of Aerospace Science and Engineering, National University of Defense Technology, Changsha 410073, China; gfdlzq@163.com (Z.L.); literature_chen@nudt.edu.cn (Y.C.)

² National Innovation Institute of Defense Technology, Academy of Military Sciences, Beijing 100071, China; liuhw05@163.com (H.L.); yiyong_h@sina.com (Y.H.)

* Correspondence: zxstudy@nudt.edu.cn (X.Z.); chenxiaoqian@nudt.edu.cn (X.C.)

Received: 22 January 2020; Accepted: 18 February 2020; Published: 20 February 2020



Abstract: A foldable pneumatic soft manipulator, which has the foldability to switch between a contraction state and an expanded state, is proposed in this investigation. The soft manipulator is a structure composed of pneumatic actuators and inflatable straight arms. The directional movement is driven by the pneumatic actuators and the foldability is realized by the inflatable straight arms. Based on this design, the kinematic model of one foldable pneumatic module is developed and presented. The shape deformation and workspace of the pneumatic module is numerically calculated and analyzed. To validate the correctness of the kinematic model, the prototype of one foldable pneumatic module, as well as the relevant pneumatic control system, is designed and developed. The repeatability of the pneumatic module and the model prediction accuracy are tested and validated by the experiment.

Keywords: soft manipulator; pneumatic; foldable; kinematic model; experiment

1. Introduction

Soft manipulators are an important type of soft robot, which have become a research focus in recent years [1,2]. In messy and crowded environments, such as a mine site, or scientific exploration, the collision between the traditional rigid manipulator and the environment may damage the scene, causing a secondary disaster [3]. Thus, the soft manipulator shows a good supplementary application. In space manipulation, the space manipulator was firstly installed on the space shuttle in 1980s. Traditional space manipulators have a large volume and weight, which results in a great challenge and a high cost to the rocket [4,5]. If the space manipulator can be folded into a small volume with a light weight before launch, it will definitely have a much greater prospect in space missions. Moreover, this kind of foldable pneumatic manipulator will also have a wide application in future industrial fields, physical human–robot interactions, and many other fields. For example, the ultralight pneumatic arm with a long range can be used in disaster rescue and home or healthcare applications [6–8]. It can also work in underwater environments just like a soft electronic fish [9,10]. In confined spaces, where traditional rigid equipment cannot work, the pneumatic soft manipulator shows competent performance [11–14].

Currently, pneumatic soft manipulators have been developed rapidly. There are several kinds of typical prototypes presenting in the literature reports. Grissom et al. [15–17] designed and developed the octopus-inspired OctArm series of soft robot manipulators, each of which is constructed using air muscle extensors with three control channels per section that provide two axes bending and extension. Falco et al. [18,19] presented a soft manipulator for minimally invasive surgery (MIS) inspired by the

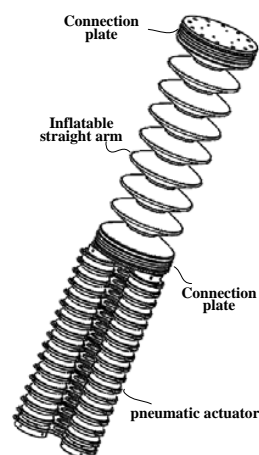
biological capabilities of the octopus arm, which was composed of three identical fluidic actuators allowing omnidirectional bending and elongation. Vosembert et al. [20–22] presented a design of a soft manipulator, which used one whole bellows as the main structure and was driven by a series of cables. Kim et al. [23] designed a pneumatic soft manipulator composed of an inflatable structure, which was entirely composed of plastic film. Sanan et al. [7,24] proposed a design scheme of an inflatable robotic arm that could generate a twisting motion. Qi et al. [25,26] proposed an inflatable soft manipulator controlled by cables. Ishibashi et al. [27] proposed a design scheme of a pneumatic arm that used pneumatic bellows as the driving actuator. Al-Ibadi et al. [28] presented a design of a continuum arm, which has the ability to extend and bend, based on McKibben pneumatic muscle actuators (PMA). Khin et al. [29] presented fabric-based soft robotic modules composing of an inflatable beam and fabric-based rotary actuator, which was designed with origami-inspired V-shaped pleats. Zhang et al. [30] proposed a mechatronics-embedded soft module powered via a single air tube due to an air supply sharing design. In these above investigations, the pneumatic manipulators are driven by pressured air or cables. The focus is mainly on the design and fabrication of the pneumatic actuators without considering the foldability of the manipulator, which is an important factor to its application in confined storage environments, such as applications in space and underwater.

In this paper, a pneumatic soft manipulator with the foldability to switch between a contraction state and an expanded state is designed and developed. In the second part, the design schematic of the soft manipulator is proposed, and the kinematic model of one foldable pneumatic module is developed. In the third part, the numerical results, including the shape deformation and the workspace of the soft manipulator, are obtained and analyzed. In the fourth part, the experimental system is designed and developed. The repeatability of the pneumatic module and the prediction accuracy of our proposed model are tested and validated. Finally, the conclusions are given in the fifth part.

2. Kinematic Modelling of the Foldable Pneumatic Soft Manipulator

2.1. Design Schematic

The foldable pneumatic soft manipulator is designed to have the foldability in its volume. When it is evacuated, the soft manipulator is in a contraction state, which can greatly save the storage space. When it is inflated, the soft manipulator can switch to an expanded state, which can result in a large workspace. This kind of foldability is realized by a structure composed of several foldable pneumatic modules which are all standardized and identical. The design of a foldable pneumatic module is shown in Figure 1.



(a) The overview design of the foldable pneumatic module.

Figure 1. Cont.

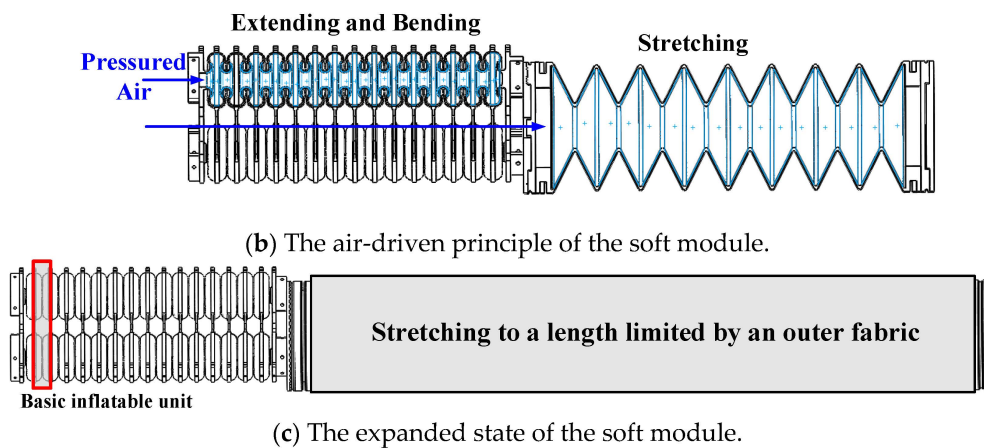


Figure 1. Design of the foldable pneumatic module.

In Figure 1a, it is seen that the foldable pneumatic module is composed of a pneumatic actuator, an inflatable straight arm, as well as the connection plate between the two parts. The pneumatic actuator is made up of three parallel and symmetric inflatable bellows, which are connected by a series of rigid constraint plates. The straight arm adopts a two-level structure, the inner level and the outer level. The inner level is a bellows made of silicone rubber, which is flexible and is responsible for the sealing. The outer level is a cylinder beam made of nylon fabric, which limits the lateral and longitudinal expansion of the inner silicone rubber. In Figure 1b, the air-driven principle of the soft module is shown. The pressured air is inputted into the inflatable bellows and the inflatable straight arm independently. The pneumatic actuator can make the directional motion when the air pressure is different in the three bellows. The inflatable straight arm can switch between a compact state and an expanded state when the pressured air is evacuated or filled. In Figure 1c, the expanded state of the soft module is shown. The total length of the inflatable straight arm is limited by the outer level fabric. The directional movement of the pneumatic actuator is the bending accumulation of a large number of basic inflatable units. By controlling the movement of the pneumatic actuator, the motion control of the soft manipulator can be realized.

2.2. Kinematic Model of the Foldable Pneumatic Module

The foldable pneumatic module, which includes a pneumatic actuator and an inflatable straight arm, is the basic unit of the pneumatic soft manipulator. The difficulty to model the kinematic performance of the pneumatic module lies in the pneumatic actuator. To develop the kinematic model of the pneumatic actuator, a basic inflatable unit is taken and shown in Figure 2. The inflatable unit is composed of three bellows slices that are arranged in an equilateral triangle configuration, and its upper and lower ends are fixed together by rigid constraint plates. It is assumed that the lower end is fixed and the upper end can move freely.

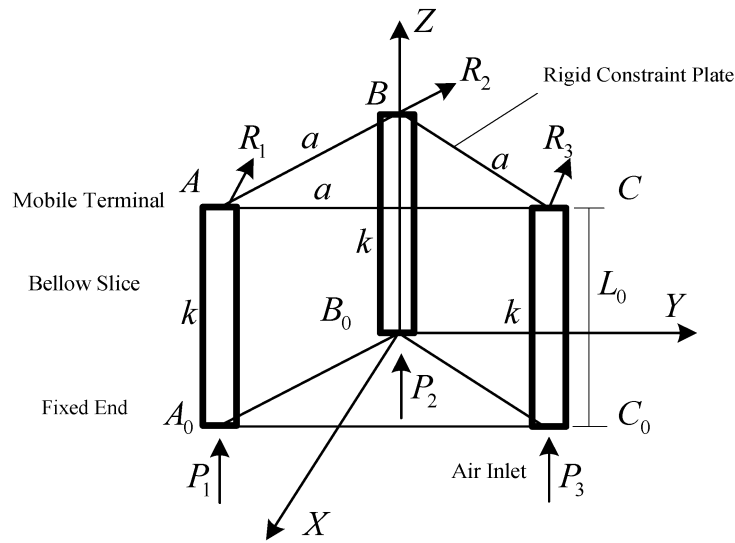


Figure 2. Basic inflatable unit of the pneumatic actuator.

As is shown in Figure 2, the basic inflatable unit is just a small slice taken from the whole pneumatic actuator. The length of the equilateral triangle configuration is a . When the bellows are not inflated, the bellows slice remains its original length L_0 . Once the bellows are inflated, the bellows stretches along the axial direction. The elongation of the manipulator is produced by the extension of the bellow structure. Therefore, the strain of the bellow still agrees with the small deformation assumption. Moreover, the axial elongation of the bellows is considered, while the radial inflation is neglected. For the convenience of analysis, the elongated cylindrical bellows is considered as an elastomer. It is assumed that the elastic coefficients of the three bellows are the same, k . The internal pressures of the three bellows are P_1 , P_2 and P_3 respectively. The forces produced by the elongation of the three bellows are F_1 , F_2 and F_3 , and the elongations are ΔL_1 , ΔL_2 and ΔL_3 respectively. When the bellows are inflated, the deformations are assumed to be in the elastic range, thus

$$\begin{cases} F_1 = k\Delta L_1 \\ F_2 = k\Delta L_2 \\ F_3 = k\Delta L_3 \end{cases} \quad (1)$$

It is assumed that the internal cross-sectional area of the bellows is S . Considering the torque balance of the rigid constraint box at the upper end, it can be obtained as follows:

$$\begin{cases} F_1 = k\Delta L_1 = P_1 S \\ F_2 = k\Delta L_2 = P_2 S \\ F_3 = k\Delta L_3 = P_3 S \end{cases} \quad (2)$$

After inflation, if there is no upper rigid constraint plate, the lengths of the three bellows are respectively:

$$\begin{cases} L_1 = L_0 + \Delta L_1 = L_0 + \frac{P_1 S}{k} \\ L_2 = L_0 + \Delta L_2 = L_0 + \frac{P_2 S}{k} \\ L_3 = L_0 + \Delta L_3 = L_0 + \frac{P_3 S}{k} \end{cases} \quad (3)$$

The mechanical effects of the rigid constraint plates at the upper end are as follows: (1) The three points A, B and C at the upper end of the three bellows keep still an equilateral triangle, and the length of the side is a ; (2) Making the normal direction of the upper plates of the three bellows point to the same direction. The forces produced by the upper rigid constraint plates on the three bellows are R_1 , R_2 and R_3 respectively, and their directions are located in the plane where the constraint plate is

located. Taking the fixed-end plane as the XY plane, a cartesian coordinate system is established, as shown in Figure 2. A_0, B_0 and C_0 are the fixed ends of the three bellows respectively. The three points constitute an equilateral triangle, and the length of the side is a . Taking the B_0 point as the origin of the coordinate, the axis x is perpendicular to the A_0C_0 downward direction, the axis y is horizontal to the right, and the axis z is perpendicular to the X-Y plane, forming a right-handed cartesian coordinate system. In this coordinate system, the coordinates of A_0, B_0 and C_0 can be written as,

$$\begin{cases} A_0 : \left(\frac{\sqrt{3}}{2}a & -\frac{a}{2} & 0 \right) \\ B_0 : \left(0 & 0 & 0 \right) \\ C_0 : \left(-\frac{\sqrt{3}}{2}a & \frac{a}{2} & 0 \right) \end{cases} \tag{4}$$

In the uninflated state, the coordinates of the A, B and C can be obtained by,

$$\begin{cases} A : \left(\frac{\sqrt{3}}{2}a & -\frac{a}{2} & L_0 \right) \\ B : \left(0 & 0 & L_0 \right) \\ C : \left(-\frac{\sqrt{3}}{2}a & \frac{a}{2} & L_0 \right) \end{cases} \tag{5}$$

Considering the effect of R_1, R_2 and R_3 , the deflections of the upper end of the three bellows are

$$\begin{cases} v_1 = \frac{R_1L_1^3}{3E_1I} = \frac{R_1L_1^2S'}{3kl} \\ v_2 = \frac{R_2L_2^3}{3E_2I} = \frac{R_2L_2^2S'}{3kl} \\ v_3 = \frac{R_3L_3^3}{3E_3I} = \frac{R_3L_3^2S'}{3kl} \end{cases} \tag{6}$$

where, E is the elastic modulus, I is the moment of inertia, EI is the bending stiffness. S' is the cross-sectional area of the wall of the bellows, that is, the effective area under axial tension. For the section of the ring whose outer diameter is R and the inner diameter is r , its moment of inertia is

$$I = \int y^2 dA = \int_0^\pi \left(\frac{R+r}{2}\right)^2 \sin^2 \theta \frac{R^2-r^2}{2} d\theta = \frac{\pi(R+r)^3(R-r)}{16} \tag{7}$$

Under the action of R_1, R_2 and R_3 , the angles generated at the upper end of the three bellows are

$$\begin{cases} \theta_1 = \frac{R_1L_1^2}{2E_1I} = \frac{R_1L_1S'}{2kl} \\ \theta_2 = \frac{R_2L_2^2}{2E_2I} = \frac{R_2L_2S'}{2kl} \\ \theta_3 = \frac{R_3L_3^2}{2E_3I} = \frac{R_3L_3S'}{2kl} \end{cases} \tag{8}$$

Considering that the endpoints on the three bellows A, B and C have the same normal direction, it means that,

$$\begin{cases} \theta_1 = \theta_2 \\ \theta_1 = \theta_3 \end{cases} \Rightarrow \begin{cases} R_1L_1 = R_2L_2 \\ R_1L_1 = R_3L_3 \end{cases} \tag{9}$$

The fact that $A, B,$ and C have the same normal orientation means that the projection of the three bellows are parallel in the X-Y plane. Supposed that the angle from the axis x counterclockwise to the projection is α , then the coordinates of the upper endpoints of the three bellows after inflation are respectively as follows:

$$\begin{cases} A' : \left(v_1 \cos \alpha + \frac{\sqrt{3}}{2}a & v_1 \sin \alpha - \frac{a}{2} & L_1 \right) \\ B' : \left(v_2 \cos \alpha & v_2 \sin \alpha & L_2 \right) \\ C' : \left(v_3 \cos \alpha + \frac{\sqrt{3}}{2}a & v_3 \sin \alpha + \frac{a}{2} & L_3 \right) \end{cases} \tag{10}$$

Under the constraint of the upper rigid plates, the distance condition satisfies,

$$L_{A'B'} = a, L_{B'C'} = a, L_{C'A'} = a \tag{11}$$

To simplify the equation, it is supposed that

$$R_1L_1 = R_2L_2 = R_3L_3 = W \geq 0, \frac{S'}{3kl} = M > 0 \tag{12}$$

It is assumed that the elongations of the three bellows are all greater than zero and less than ΔL , then there is $0 \leq \Delta L_1, \Delta L_2, \Delta L_3 \leq \Delta L$. It can be proved that the established condition of the expression $3a^2 - 3(\Delta L_1 - \Delta L_3)^2 - (2\Delta L_2 - \Delta L_3 - \Delta L_1)^2 \geq 0$ is $\Delta L/a \leq \sqrt{3}/2$, which means that the ratio of the bellow elongation to the bellow diameter is less than $\sqrt{3}/2$. Considering that the elongation of each section of the pneumatic actuator is small, the condition is satisfied in actual motion.

When $\Delta L_1 \neq \Delta L_3$, it can be gotten,

$$W = \frac{a \sin \alpha}{M(\Delta L_1 - \Delta L_3)} \pm \frac{1}{M} \text{sign}(\Delta L_1 - \Delta L_3) \times \sqrt{\frac{3a^2 - 3(\Delta L_1 - \Delta L_3)^2 - (2\Delta L_2 - \Delta L_3 - \Delta L_1)^2}{3(\Delta L_1 - \Delta L_3)^2 + (2\Delta L_2 - \Delta L_3 - \Delta L_1)^2}} \tag{13}$$

When $\Delta L_1 = \Delta L_3 \neq \Delta L_2$, the W can be expressed as

$$W = \frac{-\sqrt{3}a \cos \alpha}{M(\Delta L_1 - 2\Delta L_2 + \Delta L_3)} \pm \frac{1}{M} \text{sign}(\Delta L_1 - 2\Delta L_2 + \Delta L_3) \times \sqrt{\frac{3a^2 - 3(\Delta L_1 - \Delta L_3)^2 - (2\Delta L_2 - \Delta L_3 - \Delta L_1)^2}{3(\Delta L_1 - \Delta L_3)^2 + (2\Delta L_2 - \Delta L_3 - \Delta L_1)^2}} \tag{14}$$

The root W of the equation contains two positive solutions, the smaller one of which is the actual solution to the equation. This is because the smaller one corresponds to a small deflection which agree with the physical truth. The function of the rigid constraint plates is to ensure that the three central points of the bellows keep an equilateral triangle with a side length of a . All the flexible bellows are identical and have the same inside diameter, outside diameter, length and elasticity coefficient.

According to the symmetry, the motion of each bellow unit is the same with respect to its own coordinate system, as shown in Figure 2. Transfer the coordinate $B_0 - xyz$ to a new origin point B , and the definition of the new coordinate $x_1y_1z_1$ in the plane ABC is the same with the coordinate xyz . Then the transferring method from the coordinate $x_0y_0z_0$ to the coordinate $x_1y_1z_1$ without considering the origin shift can be written as,

$$\begin{pmatrix} x_1 \\ y_1 \\ z_1 \end{pmatrix} = \mathbf{H} \begin{pmatrix} x_0 \\ y_0 \\ z_0 \end{pmatrix} = \mathbf{M}_3(-\alpha) \mathbf{M}_2(\theta) \mathbf{M}_3(\alpha) \begin{pmatrix} x_0 \\ y_0 \\ z_0 \end{pmatrix} \tag{15}$$

where \mathbf{H} is the transferring matrix, thus

$$\begin{pmatrix} x_0 \\ y_0 \\ z_0 \end{pmatrix} = \mathbf{H}^T \begin{pmatrix} x_1 \\ y_1 \\ z_1 \end{pmatrix} \tag{16}$$

When the origin shift $\vec{B_0B_1}$ is considered, the transferring method from the coordinate $x_0y_0z_0$ to the coordinate $x_1y_1z_1$ can be written as

$$\begin{pmatrix} x_0 \\ y_0 \\ z_0 \end{pmatrix} = \mathbf{H}^T \begin{pmatrix} x_1 \\ y_1 \\ z_1 \end{pmatrix} + \vec{B_0B_1} \tag{17}$$

where $\vec{B_0B_1}$ can be obtained by combining the equations (4) and (10),

$$\vec{B_0B_1} = \left(v_2 \cos \alpha \quad v_2 \sin \alpha \quad L_2 \right)^T \tag{18}$$

By using this transferring method, the motion of the whole pneumatic actuator can be described. Assumed that the total number of the bellow slices is N in the pneumatic actuator, the coordinate of the top plane center of the pneumatic actuator is \mathbf{r}^* , then the coordinate of \mathbf{r}^* relative to the fixed coordinate system $x_0y_0z_0$ can be expressed as

$$\mathbf{r}_N = (\mathbf{H}^T)^{N-1} \mathbf{r}^* + \left[(\mathbf{H}^T)^{N-2} + (\mathbf{H}^T)^{N-3} + \dots + (\mathbf{H}^T)^1 + (\mathbf{H}^T)^0 \right] \vec{B_0B_1} \tag{19}$$

Using the above equation, the directional motion of the pneumatic actuator can be depicted. The inflatable straight arm is fixed at the end of the pneumatic actuator, and the elongation of the straight arm is in the tangent direction of the end of the pneumatic actuator. The stiffness of the straight arm with a certain air pressure can reach to a much higher level than the pneumatic actuator, thus the straight arm can be simplified as a straight line in the kinematic modelling process. Then the coordinate of the free top of the straight arm \mathbf{r}_{TS} can be obtained by

$$\mathbf{r}_{TS} = (\mathbf{H}^T)^N \begin{pmatrix} 0 \\ 0 \\ L_S \end{pmatrix} + \left[(\mathbf{H}^T)^{N-1} + (\mathbf{H}^T)^{N-2} + \dots + (\mathbf{H}^T)^1 + (\mathbf{H}^T)^0 \right] \vec{B_0B_1} \tag{20}$$

where L_S is the length of the straight arm. Until now, the kinematic model of the pneumatic soft module has been developed. The shape deformation and the workspace of the pneumatic soft module can be described and analyzed based on this kinematic model.

3. Numerical Calculation and Analysis

3.1. Model Parameters

In order to evaluate the prediction results of the kinematic model of the pneumatic module, the programming is coded in Matlab, which is a multi-paradigm numerical computing environment developed by MathWorks, an American privately held software corporation. The model parameters, as well as their values used in the numerical calculation, are listed in Table 1. L_0 is the original length of each bending unit, a is the distance between each bending unit, N is the number of bending units, d_{out} is the outer diameter of the bending unit, d_{in} is the inner diameter of the bending unit, T is the height of the bending unit, L_{empty} is the length of the straight arm in empty state, and L_{full} is the length of the inflated state. The specific parameters are adjusted according to each calculation example.

Table 1. Model parameters of pneumatic actuator and straight arm.

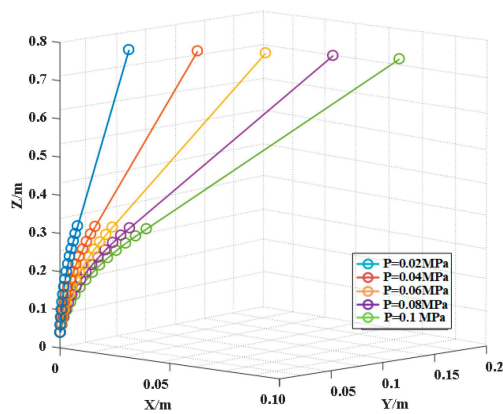
Parameter Value	L_0 0.02 m	a 0.1 m	N 16	L_{empty} 0.2 m
Parameter Value	d_{out} 0.05 m	d_{in} 0.0488 m	T 0.02 m	L_{full} 0.442 m

In the calculation process, the elastic coefficient K of the pneumatic actuator has a significant effect on the calculation results. Due to the complex structure of the pneumatic actuator, there is no theoretical formula to directly give the K value, so we need to measure it through experiment. The experimental principle is similar to the spring elastic coefficient measurement method. By measuring the relationship between the elongation and the pressure, the elastic coefficient k value of the pneumatic actuator

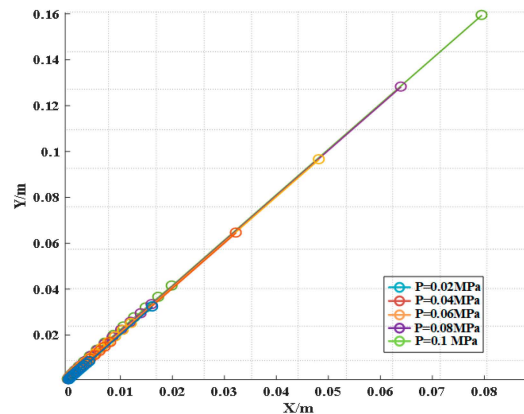
is obtained by fitting with considering the influence of gravity. Finally, in the calculation process, the elastic coefficient k value of the pneumatic actuator is given as 23,000 N/m.

3.2. Shape Deformation of the Pneumatic Module

In this calculation, the internal pressure of the straight arm is fixed at 0.025 MPa. The loading air pressure of the pneumatic actuator is taken from 0.02 MPa to 0.1 MPa, with an interval of 0.02 MPa. Firstly, we inflate one bellows; the other two bellows are not inflated. Then we inflate two bellows with the same pressure, while the other one is not inflated. The numerical results are shown in Figures 3 and 4.

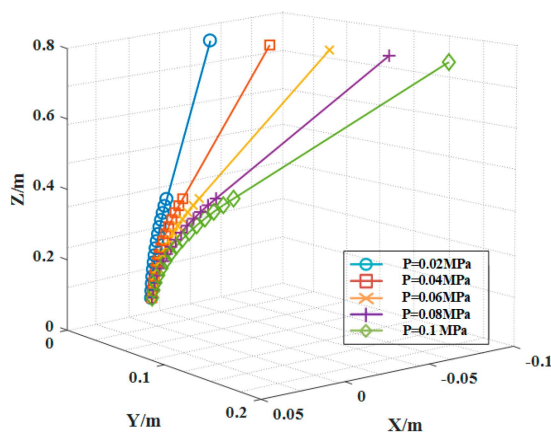


(a) Shape deformation.

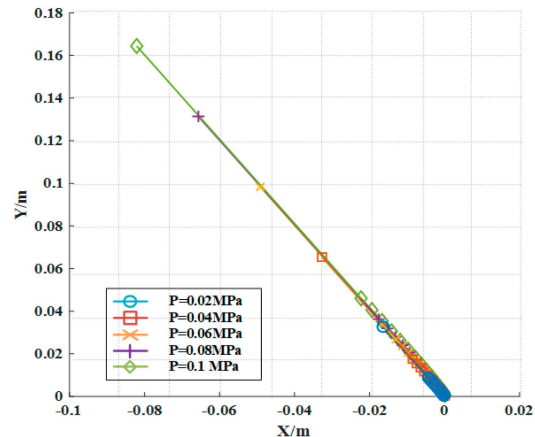


(b) Projection in the X–Y plane.

Figure 3. Space distribution of the soft manipulator with one bellows inflated.



(a) Shape deformation.



(b) Projection in the X–Y plane.

Figure 4. Space distribution of the soft manipulator with two bellows inflated.

It can be seen in Figures 3a and 4a that the shape deformation increases with the increase of the internal pressure with both one bellows and two bellows inflated. The line of the straight arm is just along the tangent direction of the end point of the pneumatic actuator. It can be seen in Figures 3b and 4b that the projection of the numerical results in the X–Y plane is a straight line, and the projections in these two situations are almost symmetric about the Y-axis. This phenomenon is consistent with the physical law, indicating that there is no singularity and disturbance occurring during the deformation process predicted by the theoretical model. From the analysis above, it is verified that the numerical

results of the theoretical model are reasonable. However, the accuracy of the shape deformation predicted by the proposed model still needs to be validated through experiment.

3.3. Workspace of the Pneumatic Module

The workspace is an important index to measure the performance of the manipulator. According to the requirements for different mission scenarios, a design scheme of combination structure is proposed. With the combination of pneumatic actuator and straight arm, the workspace of the manipulator can be increased efficiently by changing the length of the straight arm. If the manipulator only consists of a pneumatic actuator, the overall weight of the manipulator will be greatly increased. However, the combined structure of the flexible pneumatic actuator and lightweight straight arm can not only reduce the overall weight of the manipulator, but also greatly expands the workspace of the manipulator. In order to compare the workspace with or without considering the straight arm, two examples are numerically calculated based on the proposed model of the soft manipulator. In these two examples, the three bellows are inflated from 0.01 MPa to 0.1 MPa randomly, and the maximum workspaces with or without considering the straight arm are obtained and shown in Figure 5.

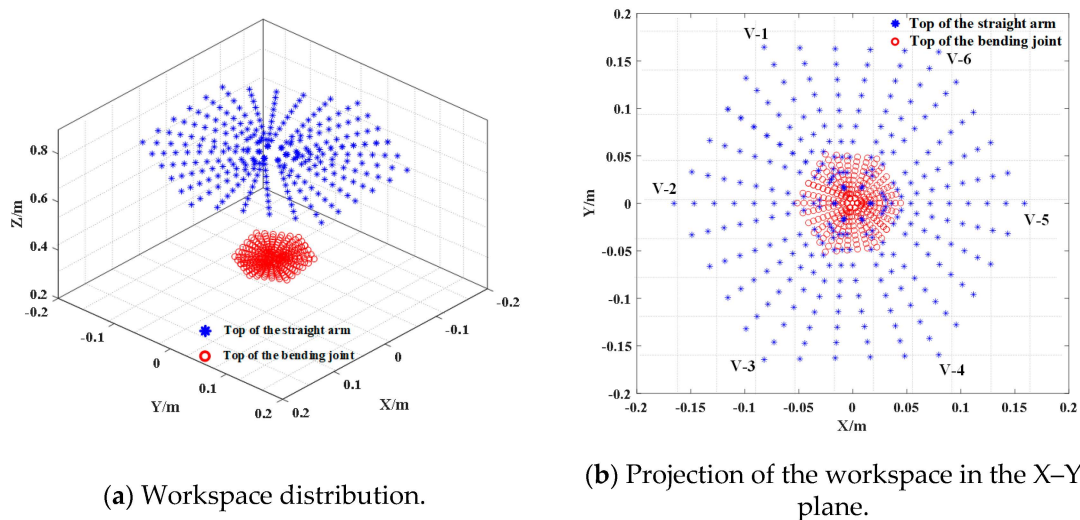


Figure 5. Workspace of the end point of the soft manipulator.

In Figure 5, the arc surface marked with blue stars represents the workspace of the combination structure of straight arm and pneumatic actuator, while the arc surface marked with red circles represents the workspace of the pneumatic actuator alone. Figure 5a shows the comparison of the two kinds of workspace in 3D view; Figure 5b shows the projection of the two workspaces in X–Y plane. From these comparisons in different views, it can be clearly known that the straight arm extends the workspace of the soft manipulator largely. It can be seen in Figure 5a that the projection of the workspace in the X–Y plane is almost hexagonal. The boundary of the hexagon is limited by the maximum internal pressures of the three bellows, which are limited in 0.1 MPa in these two numerical examples. The air pressures of the six vertices are shown in Table 2.

Table 2. The air pressures of the six vertices.

	Vertices					
	V-1	V-2	V-3	V-4	V-5	V-6
Pressure in bellow-1 (MPa)	0.1	0.1	0.1	0	0	0
Pressure in bellow-2 (MPa)	0.1	0	0	0	0.1	0.1
Pressure in bellow-3 (MPa)	0	0	0.1	0.1	0.1	0

4. Experiment Design and Validation

4.1. Experiment Design

The prototype of the foldable pneumatic module is made up of a pneumatic actuator and a straight arm. The pneumatic actuator is fabricated by selective laser sintering (SLS) 3D printing technology with nylon composite powder. It consists of three independent inflatable bellows. The two sides of the pneumatic actuator are fixed by two rigid constraint planes to ensure the three bellows remain in the same plane. The straight arm consists of an inner soft retractable bellows and an outer skin. The outer skin is made of soft fiber fabric which can protect the inner soft bellows and limit the elongation of the inner bellows. The straight arm is in a contracted state when it is not inflated; after inflation, the inner bellows stretches axially to a fixed length limited by the outer skin, as shown in Figure 6.

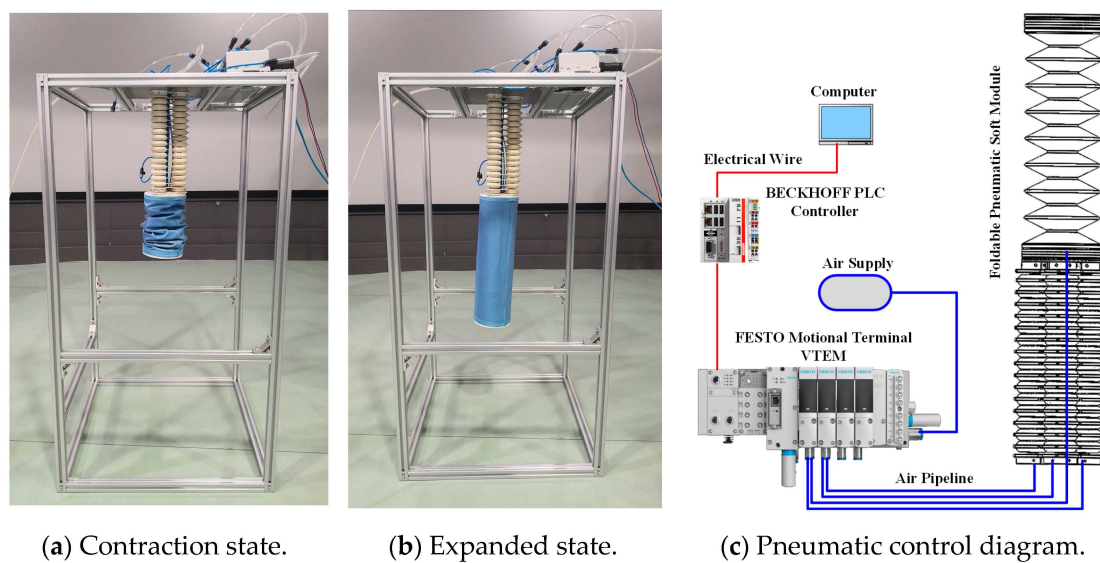


Figure 6. Prototype of the foldable pneumatic soft module.

In Figure 6a,b, the contraction state and the expanded state of the pneumatic soft module are shown respectively. In Figure 6c, the diagram of the pneumatic control system is shown. The pneumatic control system includes a Festo motion terminal VTEM, a BECKHOFF PLC controller, a computer, an air supply, electrical wires, and air pipelines. VTEM is able to control eight pipelines at a proportional pressure with four piezo pilot valves integrated in a valve terminal. The CX9020 BECKHOFF PLC controller is used to offer multi-pipelines air pressure control for the VTEM. The experimental system consists of a pneumatic control system, a measurement system, and a pneumatic soft module, as shown in Figure 7a. The measurement system includes an electronic total station and a force gauge system. On the soft manipulator, nine observation points are set and recorded in order to obtain the shape deformation of the total soft module. Five observation points are on the pneumatic actuator with equal distance, while four observation points are on the straight arm, as shown in Figure 7b. The positions of the nine observation points are recorded by using the electronic total station. The position and status of the pneumatic actuator can be obtained through measuring the position of the five observation points. The number 6 observation point is set at the junction of the pneumatic actuator and the straight arm, which is the starting point of the straight arm. Two observation points are set in the middle section of the straight arm, and one observation point is arranged at the end of the straight arm. The position and status of the straight arm can be obtained through measuring the position of the four observation points.

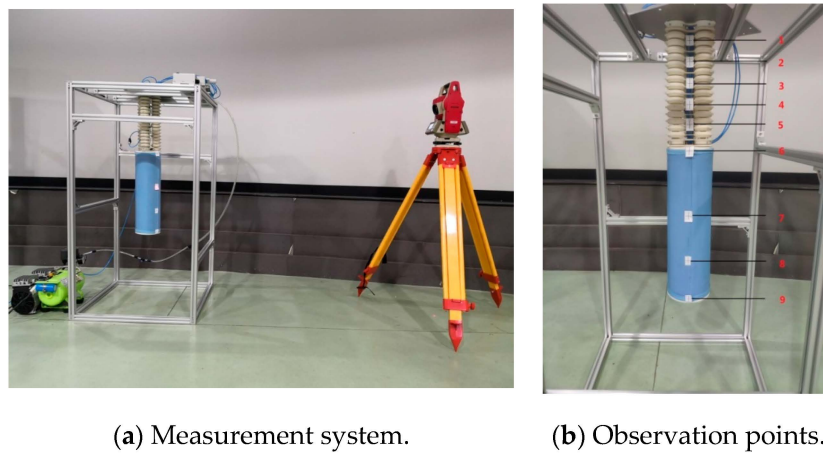


Figure 7. Experiment system of one pneumatic module.

4.2. Repeatability Test of the Pneumatic Module

In order to verify the repeated positioning accuracy of the soft manipulator, repeated experiments are taken in different working conditions. Experiments under the same working condition are taken three times, and the coordinates of the observation points are recorded. By comparing the difference of the coordinates of the same observation point in three experiments, the repeated positioning accuracy of the pneumatic soft module is tested. Experiments are taken in two conditions: one bellows inflated or two bellows inflated simultaneously.

(1) Repetition experiment with one bellows inflated

First, one bellows is inflated, and the internal pressure is set from 0.02 MPa to 0.1 MPa, with 0.02 MPa as the interval. The coordinates of the observation points are recorded, respectively. In each test, the air in the bellows is vented and then inflated. The experimental results are shown in Figure 8.

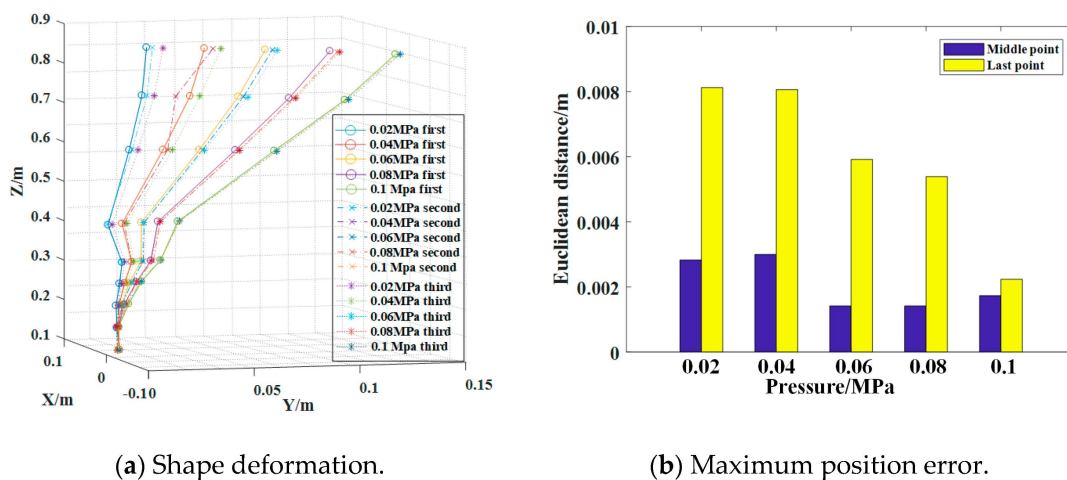


Figure 8. Repetition experiment with one bellows inflated.

In Figure 8a, the curves agree well with each other at the same internal pressure in the three experiments. As the internal pressure increases, the curves are almost completely coincided. It can be seen in Figure 8a that there is a slight difference between the three curves at a pressure of 0.02 MPa, as the internal pressure increases and the difference becomes smaller. The curves are almost completely coincident at the internal pressure of 0.1 MPa. This indicates that the stability of the soft module improves when the pressure increases. As shown in Figure 7b, the observation point number 6 is

the end point of the pneumatic actuator, and the observation point number 9 is the end point of the straight arm. These two points are taken as calibration points to obtain the maximum position errors in the three measurements. As can be seen in Figure 8b, the maximum error of the repeated positioning accuracy of the two calibration points is no more than 8 mm, and the repeated positioning accuracy improves with the increasing of the internal pressure. When the internal pressure increases to 0.1 MPa, the position error can be limited within 2 mm.

(2) Repeatability experiment when two bellows are inflated

We then inflated two bellows with the same internal pressure after the pneumatic soft module restores to its original state, and the internal pressure is set from 0.02 MPa to 0.1 MPa, with 0.02 MPa as the interval. The observation process is the same as the experiment with one bellows inflated. The experiment results are shown in Figure 9.

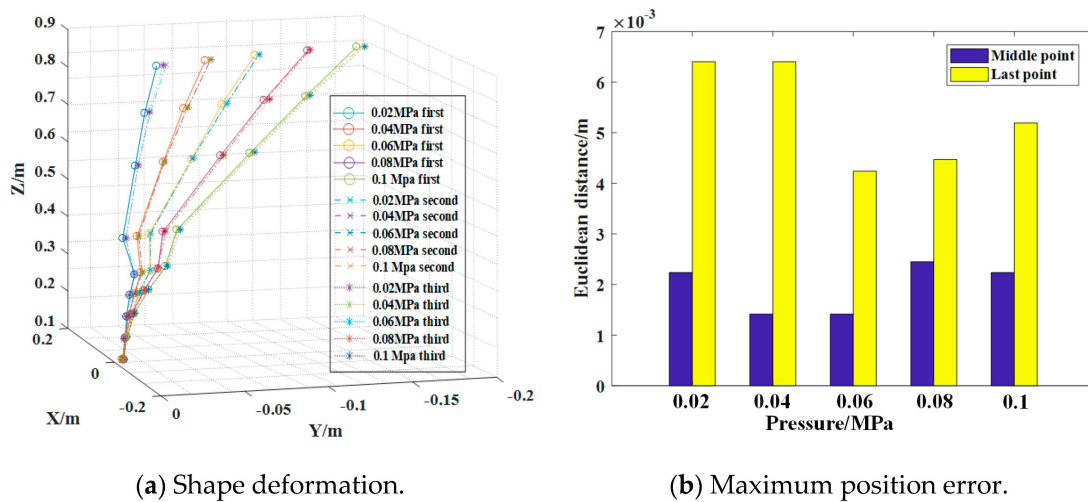


Figure 9. Repeatability experiment when two bellows are inflated.

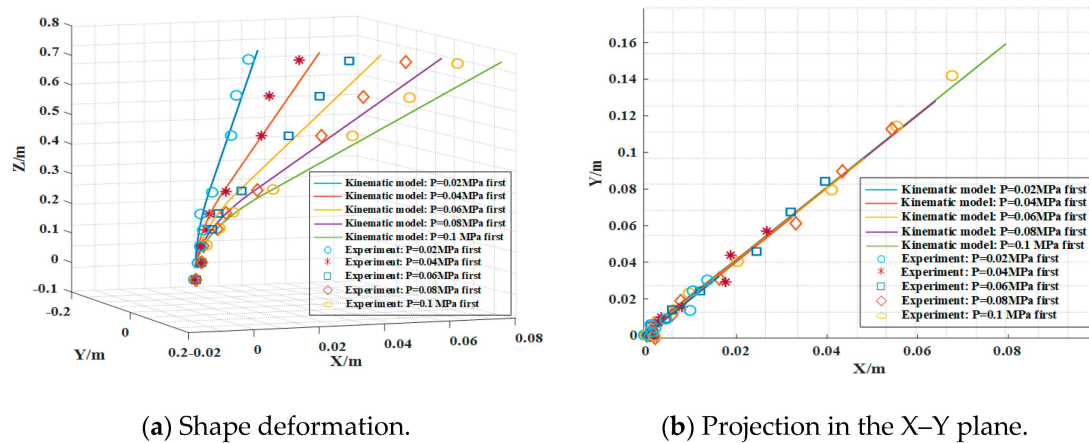
In Figure 9a, the curves almost totally agree with each other at the same internal pressure in the three experiments. The difference between the curves in the same internal pressure condition is very small, no matter the internal pressure is low or high. Similarly, observation points 6 and 9 are taken as calibration points. It can be seen in Figure 9b, the maximum position error of the number 9 observation point is about 6 mm; the maximum position error of the number 6 observation point is about 2 mm. It can be seen from the comparison between Figures 8b and 9b that the repeated positioning accuracy improves with the increasing of the internal pressure in the scenario where one bellows is inflated, while the repeated positioning accuracy is stable in the scenario where two bellows are inflated. This is because, when two bellows are inflated at the same time, the bending force generated by pneumatic actuator is greater than that of one bellows, the stability of the pneumatic soft module is also better. This can be seen in Figures 8 and 9, where the maximum error of the repeatability experiment is 8 mm, which is less than 1.5% relative to the total length of the pneumatic soft module (762 mm).

4.3. Validation of the Model Prediction Accuracy

In order to verify the accuracy of the shape deformation predicted by the proposed model, experiments are taken in different working conditions and the numerical results are compared with the experimental results. The coordinates of the observation points are recorded in the experiments in two conditions: one bellows inflated or two bellows inflated simultaneously. The coordinates of the observation points are projected into the Y-Z plane and the X-Y plane to see the difference between the modelling prediction and the experiment measurement clearly.

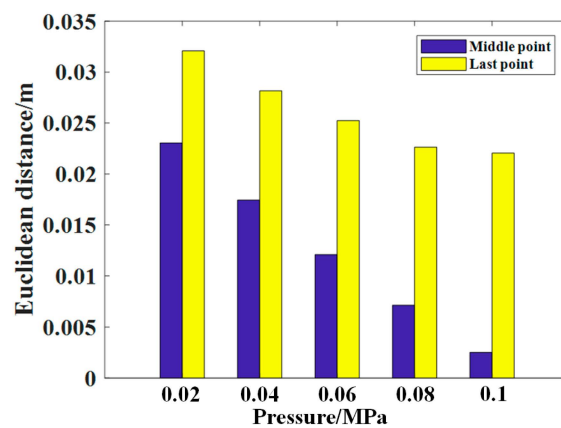
(1) Experiment with one bellows inflated

First, one bellows is inflated, and the internal pressure is set from 0.02 MPa to 0.1 MPa, with 0.02 MPa as the interval. The coordinates of the observation points are recorded respectively. In this theoretical prediction, the k value is taken as 23,000 N/m; the length of the straight arm is 0.442 m. Observation points 6 and 9 in Figure 7b are taken as calibration points to obtain the errors between the theoretical prediction results and experiment results. The coordinates of these two points are extracted at different internal pressure and compared with the prediction results. The theoretical prediction results and experiment results are compared in Figure 10.



(a) Shape deformation.

(b) Projection in the X–Y plane.



(c) Error between prediction and experiment results of calibration points.

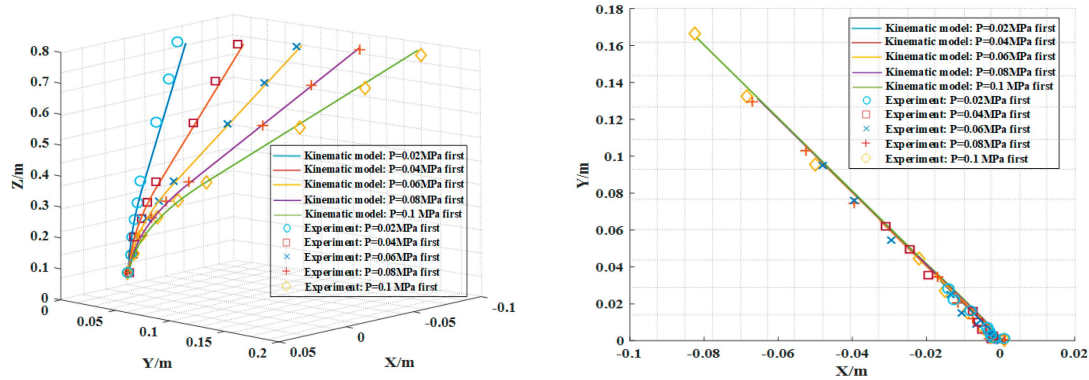
Figure 10. Comparison between prediction and experiment results of one bellows.

In Figure 10a, the shape deformations of the soft module obtained by both experiment and numerical prediction are shown. It can be seen that the distribution of experiment points is almost around the theoretical prediction. When the curves and points are projected into the X–Y plane, the theoretical results merge into a straight line and the experiment points stay around the straight line, as shown in Figure 10b. This indicates that the pneumatic soft module deforms stably in a single direction under the condition of one bellows inflated, and there is no obvious deviation occurring in the deforming process, which reflects the well stability of the pneumatic soft module. In Figure 10c, the prediction error of the theoretical model relative to the experiment is shown. It can be seen that the prediction error at both the middle point and the last point reduces with the increasing of the air pressure in the bellows. The maximum at the last point is 33 mm when the internal pressure is 0.02 MPa, and the minimum is 23 mm at the internal pressure of 0.1 MPa. The maximum and minimum at the middle point is respectively 24 mm and 2.5 mm. This is because the bending stiffness of the pneumatic joint is relatively small when the internal pressure is at a low level; thus, the bending amplitude

of the pneumatic soft module is greatly influenced by gravity. With the increasing of the internal pressure, the bending stiffness increases; thus, the influence of gravity on the bending amplitude of the pneumatic soft module reduces relatively.

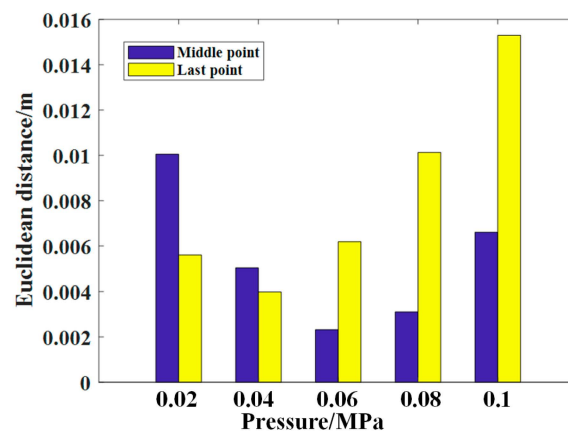
(2) Experiment with two bellows inflated

Inflating two bellows with the same internal pressure after the pneumatic soft module restores it to its original state, and the internal pressure is set from 0.02 MPa to 0.1 MPa, with 0.02 MPa as the interval. The process is the same as the experiment with one bellows inflated. The experiment results and prediction results are shown in Figure 11.



(a) Shape deformation.

(b) Projection in the X–Y plane.



(c) Error between prediction and experiment results of calibration points.

Figure 11. Comparison between prediction and experiment results of two bellows.

In Figure 11a, the shape deformations of the soft module obtained by both experiment and numerical prediction are shown. It can be seen that the distribution of experiment points is almost around the theoretical prediction. When the curves and points are projected into the X–Y plane, the theoretical results merge into a straight line and the experiment points stay around the straight line, as shown in Figure 11b. Comparing Figure 11a with Figure 10a, it can be seen that the agreement between the theoretical prediction and the experiment improves a great deal. This agreement can also be found in their projection to the X–Y plane. It indicates that the stability of the pneumatic soft module as well as the numerical prediction accuracy with two bellows inflated is far better than one bellows inflated. In Figure 11c, the prediction error of the theoretical model relative to the experiment is shown. It can be seen that the minimum prediction error at the middle point is 2 mm, appearing at the internal

pressure of 0.06 MPa. When the pressure is lower than 0.06 MPa, the prediction error reduces with the increasing of the pressure; when the pressure is higher than 0.06 MPa, the prediction error increases with the increasing of the pressure, and the maximum of the error at the last point is less than 16 mm, which is just half of that in the one-bellows condition. The reason lies in that the bending stiffness of the pneumatic joint is strengthened when two bellows are inflated. As a consequence, the stability of the pneumatic soft module improves a great deal and the influence of gravity is relatively small. However, due to the limitations of 3D printing technology, the internal structure of each bellows may not be totally identical. When the internal pressure is lower than 0.06 MPa, the elongation and deformation of the two inflatable bellows are almost identical. When the pressure is higher than 0.06 MPa, the difference in the internal structure of the two bellows is enlarged, leading to an increasing of the prediction error.

5. Conclusions

In this paper, a design of a foldable pneumatic soft manipulator composed of pneumatic actuators and inflatable straight arms was presented. The pneumatic actuators were driven by pressured air and the inflatable straight arms could switch between the contraction state and the extended state. The foldability of the soft manipulator was realized by the inflatable straight arms. Based on this design, the kinematic model of one foldable pneumatic module was proposed. From the numerical results of the shape deformation and the workspace, it can be determined that the prediction of the proposed model was reasonable. In order to validate the design and the theoretical model, an experiment system including a prototype of pneumatic soft module, a pneumatic control system, and an electronic total station was developed. Through the experiment, the repeatability of the pneumatic soft module was tested and the model prediction accuracy was validated. It can be determined that the performance of the pneumatic soft module was stable, especially in the condition of two bellows inflated. The prediction of the shape deformation by the proposed model was validated by the experimental results, although the error still existed obviously under some conditions. Based on the modelling method presented in this paper, the kinematic model of the soft manipulator composed of several pneumatic modules could be developed. Due to the advantage of the foldability, the foldable pneumatic soft manipulator will show a wide application prospect in the aerospace field in the future. In our future work, a soft manipulator composed of three pneumatic modules will be designed and developed. The experiment will be conducted based on the air floating platform, which can provide a free moving environment for the planar motion of the soft manipulator.

Author Contributions: Conceptualization, X.Z. and Y.H.; Formal analysis, H.L. and Y.C.; Funding acquisition, X.Z. and X.C.; Investigation, Y.C.; Methodology, Z.L., X.Z. and Y.H.; Validation, H.L.; Writing—original draft, Z.L.; Writing—review & editing, Y.H. and X.C. All authors have read and agreed to the published version of the manuscript.

Funding: This research was funded by the Postdoctoral Research Foundation of China and the Natural Science Foundation of China, under grant numbers 11702320, 91741107, and 11725211.

Conflicts of Interest: The authors declare no conflict of interest.

References

1. Laschi, C.; Mazzolai, B.; Cianchetti, M. Soft robotics: Technologies and systems pushing the boundaries of robot abilities. *Sci. Robot.* **2016**, *1*, eaah3690. [[CrossRef](#)]
2. Rus, D.; Tolley, M. Design, fabrication and control of soft robots. *Nature* **2015**, *521*, 467–475. [[CrossRef](#)] [[PubMed](#)]
3. Wang, H.; Zhang, R.; Chen, W.; Liang, X.; Pfeifer, R. Shape Detection Algorithm for Soft Manipulator Based On Fiber Bragg Gratings. *IEEE Asme Trans. Mechatron.* **2016**, *21*, 2977–2982. [[CrossRef](#)]
4. Jacobstein, N.; Bellingham, J.; Yang, G.Z. Robotics for space and marine sciences. *Sci. Robot.* **2017**, *2*. [[CrossRef](#)]
5. Chien, S.; Wagstaff, K.L. Robotic space exploration agents. *Sci. Robot.* **2017**, *2*, eaan4831. [[CrossRef](#)]

6. Goodrich, M.A.; Schultz, A.C. Human–robot interaction: A survey. *Found. Trends® Hum. Comput. Interact.* **2008**, *1*, 203–275. [[CrossRef](#)]
7. Sanan, S. Soft inflatable robots for safe physical human interaction. Ph.D. Thesis, Carnegie Mellon University, Pittsburgh, PA, USA, 2013.
8. Sheridan, T.B. Human–robot interaction: Status and challenges. *Hum. Factors* **2016**, *58*, 525–532. [[CrossRef](#)] [[PubMed](#)]
9. Li, T.; Li, G.; Liang, Y.; Cheng, T.; Dai, J.; Yang, X.; Liu, B.; Zeng, Z.; Huang, Z.; Luo, Y. Fast-moving soft electronic fish. *Sci. Adv.* **2017**, *3*, e1602045. [[CrossRef](#)] [[PubMed](#)]
10. Marchese, A.D.; Onal, C.D.; Rus, D. Autonomous soft robotic fish capable of escape maneuvers using fluidic elastomer actuators. *Soft Robot.* **2014**, *1*, 75–87. [[CrossRef](#)] [[PubMed](#)]
11. Marchese, A.D.; Tedrake, R.; Rus, D. Dynamics and trajectory optimization for a soft spatial fluidic elastomer manipulator. *Int. J. Robot. Res.* **2016**, *35*, 1000–1019. [[CrossRef](#)]
12. Mazzolai, B.; Margheri, L.; Cianchetti, M.; Dario, P.; Laschi, C. Soft-robotic arm inspired by the octopus: II. From artificial requirements to innovative technological solutions. *Bioinspir. Biomim.* **2012**, *7*, 25005. [[CrossRef](#)] [[PubMed](#)]
13. Onal, C.D.; Rus, D. Autonomous undulatory serpentine locomotion utilizing body dynamics of a fluidic soft robot. *Bioinspir. Biomim.* **2013**, *8*, 26003. [[CrossRef](#)] [[PubMed](#)]
14. Tolley, M.T.; Shepherd, R.F.; Mosadegh, B.; Galloway, K.C.; Wehner, M.; Karpelson, M.; Wood, R.J.; Whitesides, G.M. A resilient, untethered soft robot. *Soft Robot.* **2014**, *1*, 213–223. [[CrossRef](#)]
15. Walker, I.D.; Green, K.E. Continuum Robots. In *Encyclopedia of Complexity and Systems Science*; Meyers, R., Ed.; Springer: New York, NY, USA, 2009; pp. 1475–1485.
16. McMahan, W.; Chitrakaran, V.; Csencsits, M.; Dawson, D. Field trials and testing of the OctArm continuum manipulator. In Proceedings of the IEEE International Conference on Robotics and Automation, Orlando, FL, USA, 15–19 May 2006; pp. 2336–2341.
17. Grissom, M.D.; Chitrakaran, V.; Dienno, D.; Csencsits, M.; Pritts, M. Design and experimental testing of the OctArm soft robot manipulator. In *Unmanned Systems Technology VIII*; International Society for Optics and Photonics: Orlando, FL, USA, April 2006.
18. Falco, I.D.; Cianchetti, M.; Menciassi, A. A soft multi-module manipulator with variable stiffness for minimally invasive surgery. *Bioinspir. Biomim.* **2017**, *12*. [[CrossRef](#)] [[PubMed](#)]
19. Ranzani, T.; Cianchetti, M.; Gerboni, G.; Falco, I.D.; Menciassi, A. A Soft Modular Manipulator for Minimally Invasive Surgery: Design and Characterization of a Single Module. *IEEE Trans. Robot.* **2016**, *32*, 187–200. [[CrossRef](#)]
20. Palacio, J.M.A.; Riwan, A.; Mechbal, N.; Monteiro, E.; Voisembert, S. A novel inflatable actuator for inflatable robotic arms. In Proceedings of the IEEE International Conference on Advanced Intelligent Mechatronics, Munich, Germany, 3–7 July 2017; pp. 88–93.
21. Voisembert, S.; Mechbal, N.; Riwan, A.; Aoussat, A. Design of a Novel Long-Range Inflatable Robotic Arm: Manufacturing and Numerical Evaluation of the Joints and Actuation. *J. Mech. Robot.* **2013**, *5*, 45001. [[CrossRef](#)]
22. Voisembert, S.; Riwan, A.; Mechbal, N. Numerical evaluation of a new robotic manipulator based on inflatable joints. In Proceedings of the IEEE International Conference on Automation Science and Engineering, Seoul, Korea, 20–24 August 2012; pp. 544–549.
23. Kim, H.J.; Tanaka, Y.; Kawamura, A.; Kawamura, S.; Nishioka, Y. Improvement of position accuracy for inflatable robotic arm using visual feedback control method. In Proceedings of the 2015 IEEE International Conference on Advanced Intelligent Mechatronics (AIM), Busan, Korea, 7–11 July 2015; pp. 767–772.
24. Sanan, S.; Lynn, P.S.; Griffith, S.T. Pneumatic torsional actuators for inflatable robots. *J. Mech. Robot.* **2014**, *6*, 31003. [[CrossRef](#)]
25. Qi, R.; Lam, T.L.; Xu, Y. Mechanical design and implementation of a soft inflatable robot arm for safe human-robot interaction. In Proceedings of the 2014 IEEE International Conference on Robotics and Automation (ICRA), Hong Kong, China, 31 May–7 June 2014; pp. 3490–3495.
26. Qi, R.; Lam, T.L.; Xu, Y. Kinematic modeling and control of a multi-joint soft inflatable robot arm with cable-driven mechanism. In Proceedings of the 2014 IEEE International Conference on Robotics and Automation (ICRA), Hong Kong, China, 31 May–7 June 2014; pp. 4819–4824.

27. Ishibashi, A.; Yokota, S.; Matsumoto, A.; Chugo, D.; Hashimoto, H. Inflatable arm with rigidity for safe robots—1st report: Proposal of joint structure. In Proceedings of the 2017 IEEE International Conference on Industrial Technology (ICIT), Toronto, ON, Canada, 22–25 March 2017; pp. 1461–1465.
28. Al-Ibadi, A.; Nefti-Meziani, S.; Davis, S.; Theodoridis, T. Novel Design and Position Control Strategy of a Soft Robot Arm. *Appl. Sci.* **2018**, *7*, 72. [[CrossRef](#)]
29. Khin, P.M.; Low, J.H., Jr.; Marcelo, H.A.; Yeow, C.H. Shape Programming Using Triangular and Rectangular Soft Robot Primitives. *Appl. Sci.* **2019**, *10*, 1–15.
30. Zhang, Y.; Liu, Y.; Sui, X.; Zheng, T.; Bie, D.; Wang, Y.; Zhao, J.; Zhu, Y. A Mechatronics-Embedded Pneumatic Soft Modular Robot Powered via Single Air Tube. *Appl. Sci.* **2019**, *9*, 2260. [[CrossRef](#)]



© 2020 by the authors. Licensee MDPI, Basel, Switzerland. This article is an open access article distributed under the terms and conditions of the Creative Commons Attribution (CC BY) license (<http://creativecommons.org/licenses/by/4.0/>).